Flight Testing of a Single Point Frequency Sweeping Filtered Rayleigh Scattering Probe

M. Fischer[1,*], G. Stockhausen[1], E. Burow[1], M. Beversdorff[1], A. Chacin Krist[1], T. Kemmerling[1,2], C. Willert[1]

1: Institute of Propulsion Technology, German Aerospace Center (DLR), Germany
2: now at TOPTICA Photonics, Germany
* Correspondent author: Michael.Fischer@dlr.de

Keywords: FRS, filtered Rayleigh scattering, air data sensor, in-flight, airborne, molecular scattering, single point probe, temperature, velocity, measurement, frequency sweep, laser, OADS

ABSTRACT

We present a successful in-flight application of filtered Rayleigh scattering (FRS) for temperature measurement in close proximity to the air plane using a newly developed single point, frequency sweeping probe.

The temperature measurement is of relevance in the quantification of the density required for the evaluation of velocity from Pitot-probe measurements to obtain the true air speed (TAS). Laser optical air data sensors have the potential for contactless measurements outside the aerodynamic boundary layer. They are capable of self-diagnosis of fault conditions (e.g. signal loss, increased measurement uncertainty or spectral distortion for FRS) thereby increasing the safety of the aircraft. Compared to classical probes, they are less susceptible potential icing and blockage issues. The FRS-results presented here, are the outcome of two separate flight campaigns, carried out in the Alpine region as well as in the North Sea area. Measurement data provided information on the functionality of the FRS-system under various flight and weather conditions. Furthermore, the implementation of the FRS measurement system in the aircraft is presented; application aspects and improvements are discussed. In particular, the measurement accuracy at the actually achievable measurement rate was analyzed. For straight ahead flights at constant height, temperature mean values were in good agreement with the flight data system of the DLR research aircraft Dassault Falcon 20 (D-CMET). Aiming at in-flight air data measurements, the optical FRS measurement system requires a real-time temperature sample rate of a few Hz. We demonstrate that 2 FRS spectra per second can be acquired by a newly developed method using frequency sweeps for temperature determination. The low signal intensity of cw-laser based FRS is countered using a combined transmitter/receiver optic that focusses the entire cw-laser power into one measuring point. The light backscattered from the probe volume is collected by the same optics, filtered and imaged in a confocal arrangement onto a photomultiplier. An improved and miniaturized version of the presented FRS system could be a part of a future optical air data system (OADS). However, the strength of FRS signal relative to bright ambient conditions (e.g. sunlight, cloud backscatter) must be further improved in order to be able to measure well above cloud cover. The potential for further development is foreseen even if the accuracy required for flight data systems (~0.5 K) has not yet been achieved at a temperature measurement rate of 2 Hz.

1. Introduction

In the context of the FAME (Future Air Data System Module Evaluation) project, three different laser optical measurement techniques were first set up, validated and then combined to form an optical air data system (OADS) from research systems that can be integrated into aircraft (Fig. 1) [Kliebisch et al. 2023]. The chosen techniques consisted of laser Doppler anemometry (LDA), filtered Rayleigh scattering (FRS) and tunable laser absorption spectroscopy (TDLAS).

Figure 1. DLR research aircraft Dassault Falcon 20 (D-CMET) with opened bottom flap showing circular windows for LDA and FRS (rearward, grey/black).). Image copyright: DLR / Kliebisch.

Laser optical air data sensors have the potential of self-diagnosing fault conditions (e.g. signal loss, increased measurement uncertainty and for FRS also spectral distortion), thereby increasing the safety of the aircraft. Issues such as potential icing and blocking of classical probes [Cao et al. 2017, Jäckel et al. 2020] are mitigated, preventing possible misinterpretation of false Pitot-probe readings. Techniques like FRS and LDA in particular can be integrated with optical apertures that are flush with the fuselage. This further increases operability and safety (bird strike, external damage). The following material will focus solely on the measurement principles and implementation relevant aspects of the FRS technique in the context of its application in an aircraft. For details on the in-flight application of LDA the reader is referred to [Kliebisch, Mahnke & Damm 2023].

The Filtered Rayleigh Scattering (FRS) technique uses a molecular filter to suppress laser light scattered from surfaces (geometric scattering) or particles (Mie scattering) [Doll et al. 2012] (Fig. 2). Since the scattering process relies on molecular scattering, no additional particle seeding or natural presence of particles in the measured air flow is needed. FRS allows the simultaneous measurement of temperature (density) and velocity of flows using the light scattered by gas molecules [Forkey et al. 1996, Doll 2016]. For properties of laser Rayleigh scattering in general see also the review article [Miles et al. 2001].

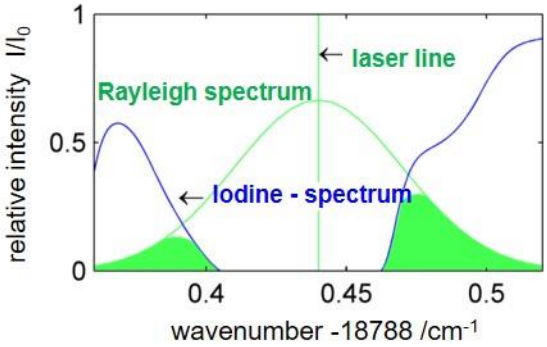

Figure 2. Principle of molecular filtering of Rayleigh scattering using the example of an iodine line. Only the green-filled (filtered) intensity ranges reach the detector.

The standard frequency scanning approach of FRS suffers from long measurement times in order of minutes, especially for planar measurements. With in-flight application in mind, air data measurements at much higher data rates are mandatory. Here we demonstrate the acquisition of temperature data at a rate of 2 samples per second.

2. Experimental set-up

The disadvantage of FRS is the low signal intensity compared to other techniques. This situation is countered with a combined transmitter/receiver optic that focusses the entire laser power into one measuring point and images the backscattered and filtered Rayleigh light in a confocal arrangement onto a photomultiplier (Fig. 3) [Jungmann (2019), Fischer et al. (2024)].
The arrangement of the associated components is shown in Fig. 3. The laser beam runs downwards through the protective tube (2) and is reflected at position 3 towards the optical axis of the receiver unit. A glass plate is mounted behind the front lens of the telescope (4), which carries a small elliptical deflecting mirror on the optical axis. This mirror reflects the laser beam through a focusing front lens into the sample volume. The backscattered light is collected in the green-filled receiving cone of the front lens and imaged through the telescope in the direction of the iodine cell

(5) for signal filtering. The iodine cell is illuminated in parallel. Behind it, a narrowband filter (6) ensures daylight suppression. Finally, the light is imaged through a lens (7) onto a pinhole (8). The pinhole diameter defines the spatial resolution and suppresses background light that does not enter at the angles from the receiving cone. The photocathode of the PMT (9) is illuminated behind the pinhole.

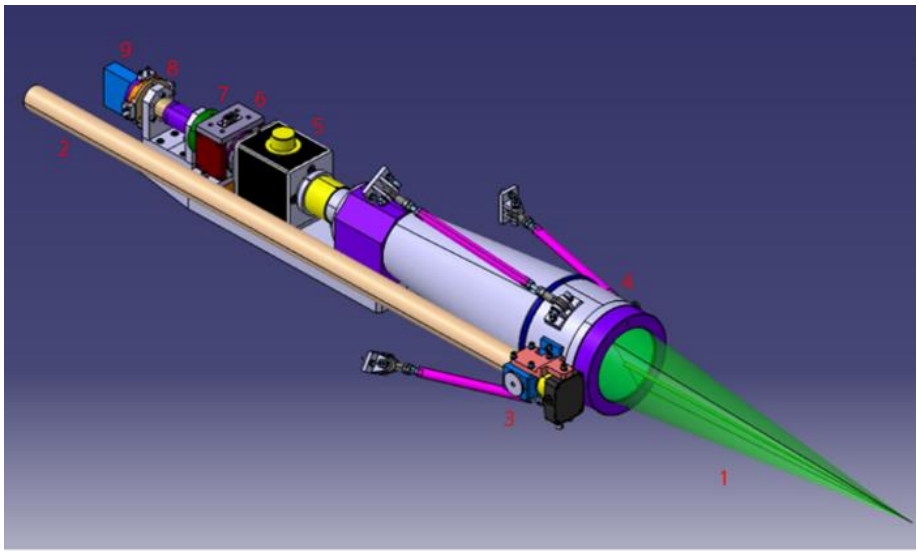

Figure 3. CAD rendering of the FRS probe (without protective housing) realized for flight tests [FAME, Fischer et al. 2024]. This picture shows the original proportions of the probe. 1: Illustration of measuring location and receiving cone. 2: Protective tube for emitted laser beam 3: Penultimate mirror deflection and diode for normalizing the signal power 4: Transmitting/receiving telescope 5: Heated Iodine cell 6: Oven controlled narrow-band filter (Aluxa, FWHM 0.25 nm) 7: Focusing lens 8: Pinhole 9: Photomultiplier

With an optimized collection angle (numerical aperture), an increase of laser power and the use of a sensitive photomultiplier, a significant signal increase could be achieved which resulted in increased temporal resolution and shortened acquisition times. A telescope with a front lens aperture of f#/5 was to produce a probe volume at a working distance of about 500 mm outside of the aircraft's boundary layer. Using a laser beam diameter of 5.5 mm a laser focus diameter of ~ 70 µm is achieved (both measured at $1/e^2$ using a beam profiler). The realized length of the FRS sample volume is about 4 mm (FWHM), using a pinhole of 300 µm.

The structure integrated into the aircraft and mounted on the seat rails consists of two flight racks containing electronics, lasers and the transceiver optics unit (Fig. 4). For the experiments presented here, we used a tunable fiber laser from (Azurlight-Systems, ALS-GR-532-6-A-SP), along with a seed-laser (NKT-Adjustik Y10) and a photomultiplier module (Hamamatsu, H9305-04). The seed-laser provides an internal triangular frequency sweep-mode which was used for the

measurements. The wavenumber sweep range was centred at about 18788.440 cm^{-1} covering the related iodine line (compare Fig. 2).

Compared to earlier work in which a diode laser-based velocimeter was used for point measurements [Jagodzinski (2007)], modern frequency-stabilized, narrow-band, high-power laser systems available today at 532 nm enable the use of iodine cells with improved laser background light suppression. This allows for an experimental configuration with numerous advantages. The single frequency laser used in the present setup provides up to 6 W green light at 532 nm with a bandwidth of less than 200 kHz. The last IR amplification fiber supplies the laser head via a flexible umbilical (left side at the top, "laser box", Fig. 4a). In the laser head the IR light is frequency-doubled to 532 nm. The emitted laser beam is then expanded to ~ 5.5 mm diameter and guided by mirrors into the transceiver system. Inside the so-called laser box, two laser shutters are used for background measurement. Finally, an iodine reference cell unit is used for frequency measurement. A total of two iodine cells are used in the system: one as filter for the FRS measurement at 70 °C saturation temperature (Fig. 3) and a reference cell for frequency determination at 25 °C saturation temperature located inside the laser box [Fischer et al. 2024]. The line transmission measurement on the 25 °C iodine cell is calibrated in advance against a wavelength meter (WLM) measurement. The housing arrangement relative to the seat rails is also shown in Fig. 4a and Fig. 4b.

The electronics rack on the right in Fig. 4a contains the components that must be directly accessible to the operator (e.g. screen and keyboard, photomultiplier electronics, shutter electronics, control electronics of the seed laser). A second rack contains additional components that do not need to be accessed during in-flight operation (e.g. computer, temperature stabilisation of the iodine cells, uninterruptible power supply for computer and other electronic components).

The vertical arrangement with laser emission downwards improves laser protection in the cabin and allows the use of a retractable floor flap to protect the optics during take-off and landing (Fig. 1). An impression of the laser emission during ground operation is shown in Fig. 5. The green emission was calculated to be eye-safe at a distance of about 41 m (6 W).

Furthermore, the FRS system is also sensitive to the vertical speed component for climb and descent. This provides additional redundancy to the classic measurement systems, if required. As a new high-quality LDA was operated in parallel during the flight tests [Kliebisch et al. 2023], the additional measure of the velocity component from FRS descent measurements so far has not been extracted from the raw FRS data. The present work concentrates on temperature measurements at constant altitude in order to minimize the number of parameters to be adjusted in the first step.

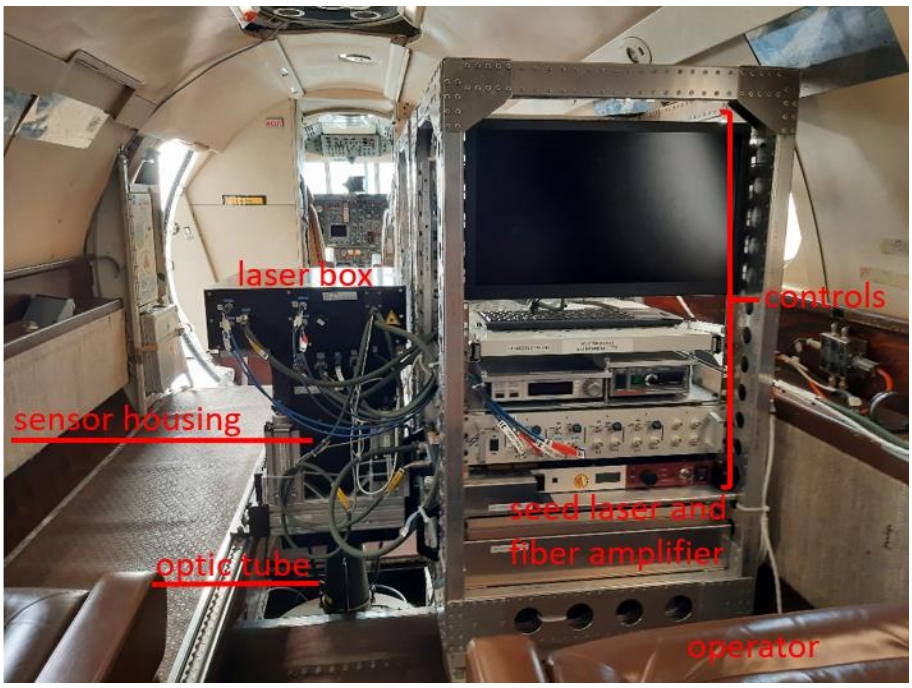

a

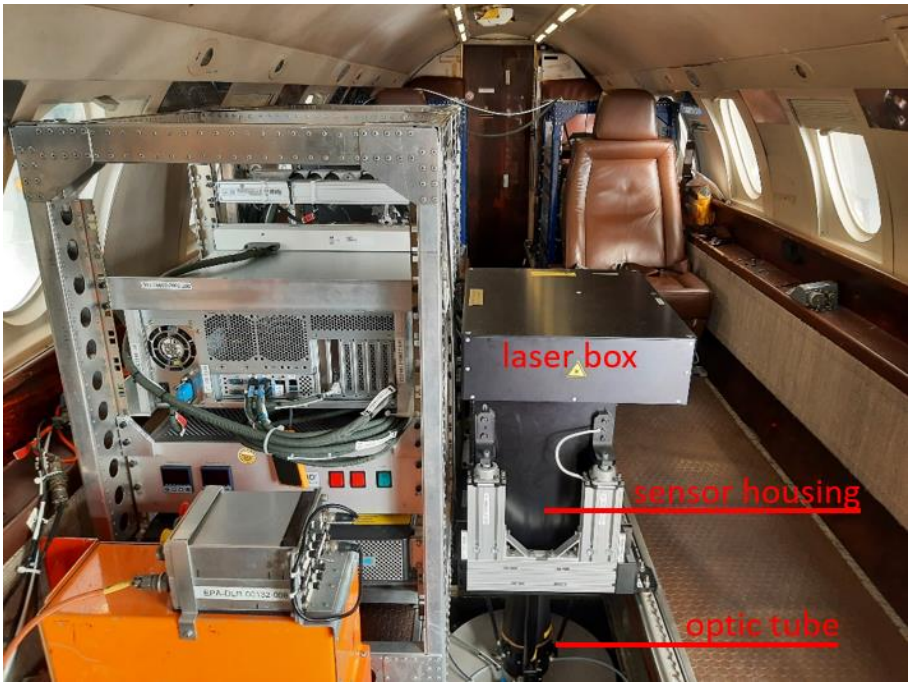

b

Figure 4. FRS system installed inside the airplane. a: View in flight direction. Rack 1 on the right. b: View against flight direction. Rack 2 on the left, laser-box, housing of FRS probe at the right.

Figure 5. FRS laser beam during ground adjustment, the central part of a larger LIDAR window is used (outer area shielded). Image copyright: DLR / Riedel.

3. Results

The two biggest effects on the success of the flight measurements turned out to be the coupling of the measurement setup to the elastic aircraft body, and the intensity and variability of the sunlight background above cloud zones. Therefore, several improvements to the setup were implemented, in particular, with regard to the mechanical stability of support structures. After optimizing the setup, a signal reduction of approx. 50% could only be seen in climb flight. The circular flights (approx. 2 G) did not affect the signal level. Due the pinhole in front of the PMT, the influence of daylight could be sufficiently reduced such that the PMT detector was not overexposed. A typical used mean FRS signal was held at about 2V PMT-Voltage, to prevent overexposure (> 10 V PMT-Voltage) at the edges of the frequency-sweep spectra due to possible cloud reflections.

For straight flight conditions the FRS data obtained at altitudes between 3000 m and 9000 m could be readily analyzed given with nearly constant daylight background and absence of strong signal interference (Fig. 6). The agreement with the static temperature (T_s) from the Falcon flight data system was 1.50 K to 2.25 K when all frequency sweeps were treated equally. The root mean square (RMS) of the individual sweep temperatures varied in the range of 3.5 K to 4.2 K (2 parameter fit of temperature T and background). With increasing altitude, the temperature drops by around 42 K (from 271.30 K to 228.87 K (T_{FRS})) while the external pressure drops by about 396 mbar (from 696.87 mbar to 300.89 mbar (P_s)). Figure 6 indicates a maintained agreement with increased height or lowered density. The temperature change of around 42 K with altitude can be

clearly recognized. The flight tests showed that the dynamic range of the measuring system makes it possible to provide reliable temperature data up to altitudes exceeding 9000 m. A temperature difference of about 2 K between T_{FRS} and T_s corresponds to only about 0.8 % of the measured value in the range between 269 K and 227 K. Average values over 10 s are analyzed here. This was done with a recording rate of two spectra per second resulting in two temperature estimates per second. The RMS scatter of the individual sweep temperatures was between 4.2 K and 5.6 K. The mean temperature agreement is similar to the ± 2 K value reported from LIDAR airborne temperature profiling in the troposphere by Rayleigh–Brillouin scattering [Witschas et al. 2021].

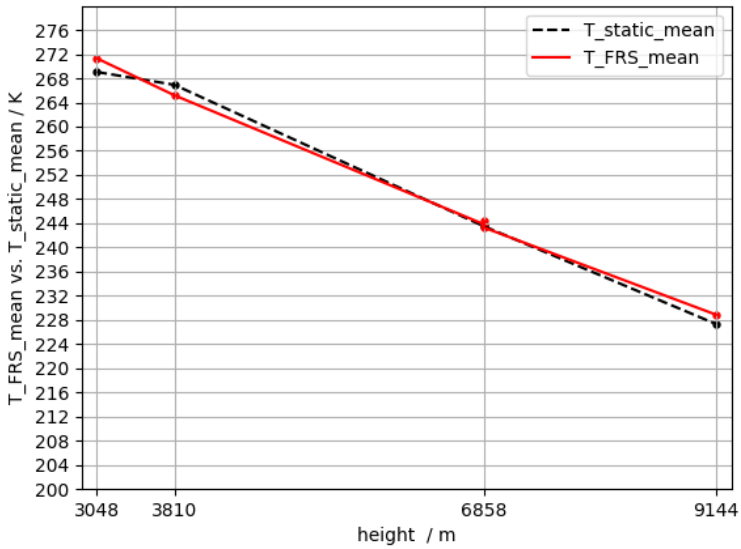

Figure 6. Mean FRS temperatures vs. mean value of the static temperature (T_s) of the Falcon flight data system in the same time window. Averaging over 10 s, 4 flight altitudes (flight level FL 100 to FL 300, 30.48 m/FL), straight flight, low sunlight background variation.

For the evaluation in this study the classical Tenti model [Doll 2016] was used, together with gas-specific parameters from [Lemmon and Jacobsen 2004]. Further information on the applicability of the Tenti S6 model to nitrogen and air is given in [Witschas 2011]. A more actual comparative analysis of evaluations using the Tenti model and analytical models, which includes work by Doll and Witschas, can be found in [Powers et al. 2022].

The repeated measurement at 6858 m (FL 225) from Fig. 6 is shown in more detail in Fig. 7. The agreement of the mean FRS temperature T_{FRS} with the mean static temperature T_s is in the range of 0.2 - 0.8 K, with corresponding RMS between 4.2 K and 5.6 K and the error of the mean between 1 K and 1.3 K. A two-parameter fit of temperature T and background parameter Ct was performed. As an example, the spectral fit of final theoretical and experimental spectrum for sweep 8 of

ensemble 1 in Fig. 7. is shown in Fig. 8. The quality corresponds to about 4 K deviation from the mean value.

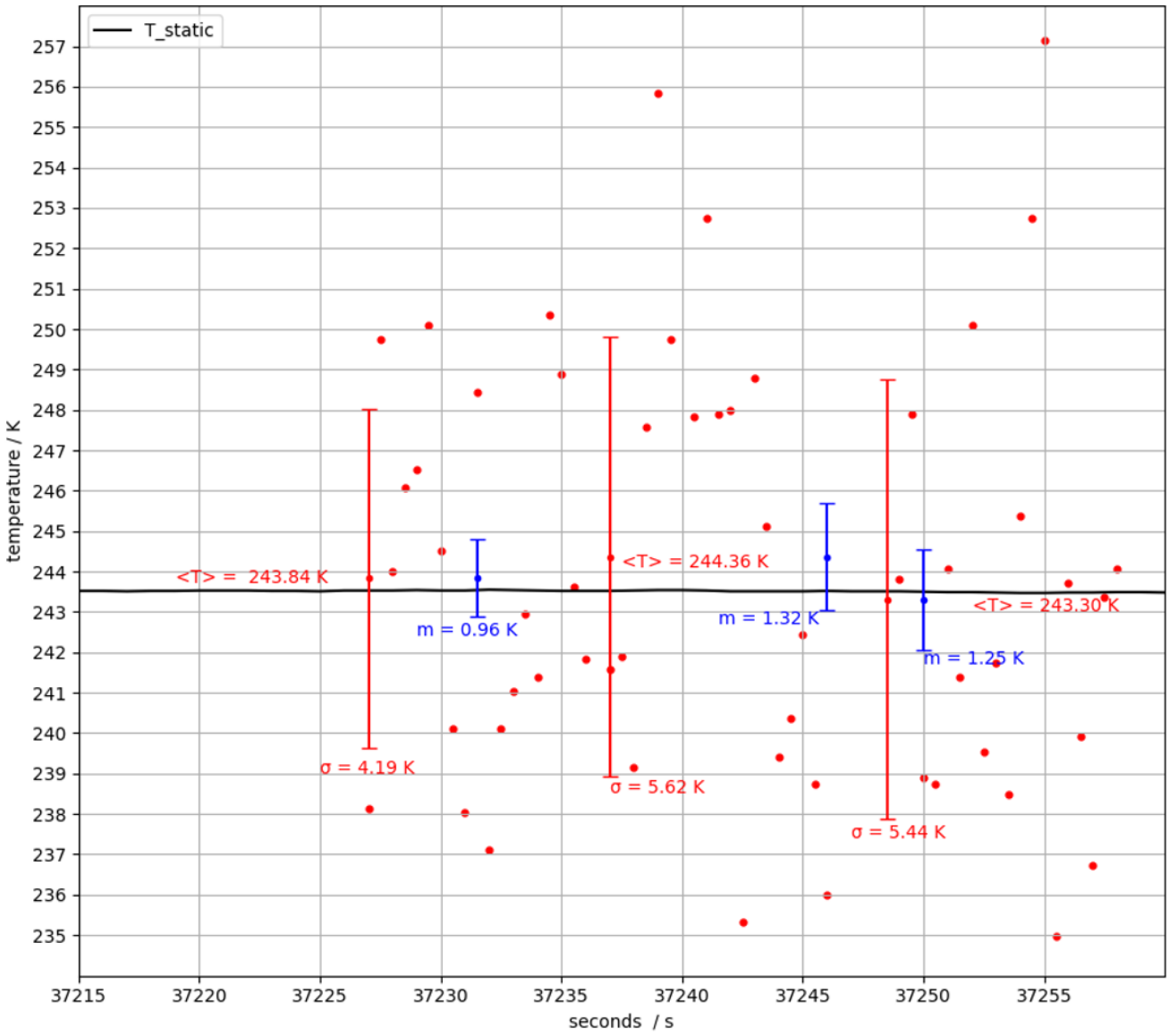

Figure 7. Single sweep temperature evaluation of three FRS data sets over in total 30 s (3x 10 s recording time, 2 spectra/s, 100 kHz raw PMT data rate, ~ 419.33 mbar, 6858 m altitude). Red and blue: FRS temperatures. Error bars represent RMS (red) and mean error of the mean (blue).

If all 56 usable sweeps of the three ensembles in Fig. 7 are evaluated together, the difference to the mean static temperature of the flight data system is further reduced to 0.1 K – 0.2 K over the sampling period of 30 s (<T_s> = 243.6 K, Fig. 9).

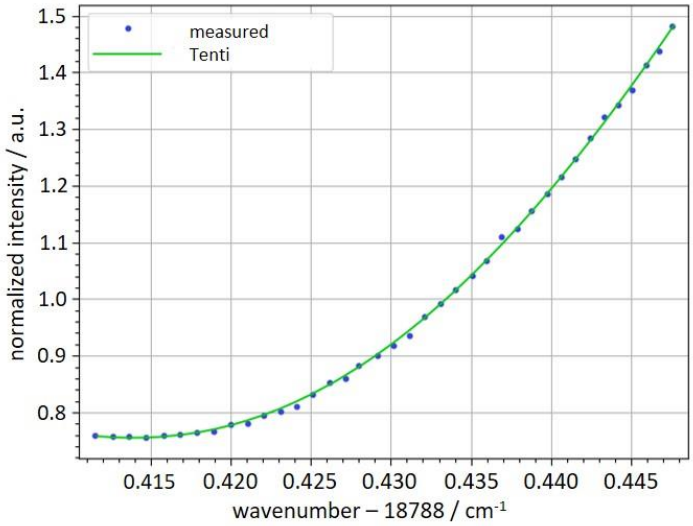

Figure 8. Final theoretical and experimental FRS-spectrum for the single sweep temperature evaluation of sweep 8 in the first ensemble Fig. 5. *T* and *Ct* were fitted.

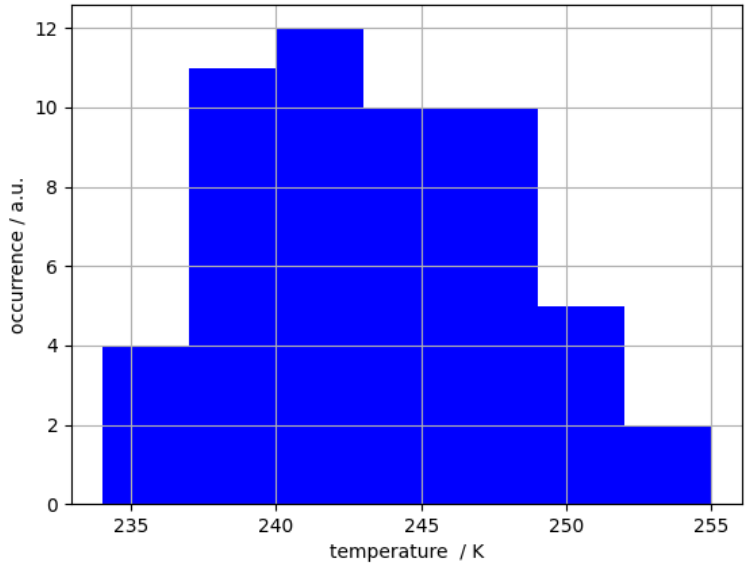

Figure 9. All data from figure 6 evaluated in one ensemble. *T* and *Ct* were fitted. Temperature occurrence per 3.0 K bin. <T_s> = 243.6 K, FRS: <*T*> = 243.8 K, *T*_median = 243.5 K

In addition to the experiments presented in straight flight, measurements were carried out at continuously varying daylight conditions. A periodically operating shutter was tested to quantify the background more frequently. A flight during evening twilight showed a reducing background signal level in the later series of measurements. Even when flying through clouds (Fig. 10), no significant influence on the signal could be detected due to the increased aerosol concentration, which was increased by orders of magnitude (Fig. 11). The background detected during cloud passage is considerably smaller than the signal levels. Only the minima are shown in the zoomed section shown together with the background level, as the edges of the spectral sweeps are greatly

exaggerated by Mie scattering but are not yet overdriven. Mie scattering can usually be suppressed by narrowing the evaluated spectral range.

Regardless of yet to be evaluated measurements involving the cyclic background sampling approach, it has been shown that there are short-term, rapid background fluctuations that cannot be resolved using only the shutter technology. The problem could be solved by installing a second, independent measuring channel that continuously detects only the background, e.g. by means of a beam splitter in front of the FRS iodine cell and a filter combination in front of the background signal detector. With such a configuration it should be possible to correctly subtract the variable background allowing system operation without or with a low background constant *Ct* correction. The temperature should then still be comparably close to the reference value, but the temperature scatter should decrease because the optimization is limited to a single parameter.

It should be noted that measurements for Fig. 6 and Fig. 7 were obtained without the periodical shutter. In this case the background signal intensity was only obtained once per 10 s measurement cycle. However, at the given constant height flight condition, the background was nearly stable as can be observed, for example, for number 30000 to 36000 in Fig. 11.

Figure 10. Cloud passage. The photo was taken during the measurement shown in Fig. 11 and shows the typical density of the clouds being flown through.

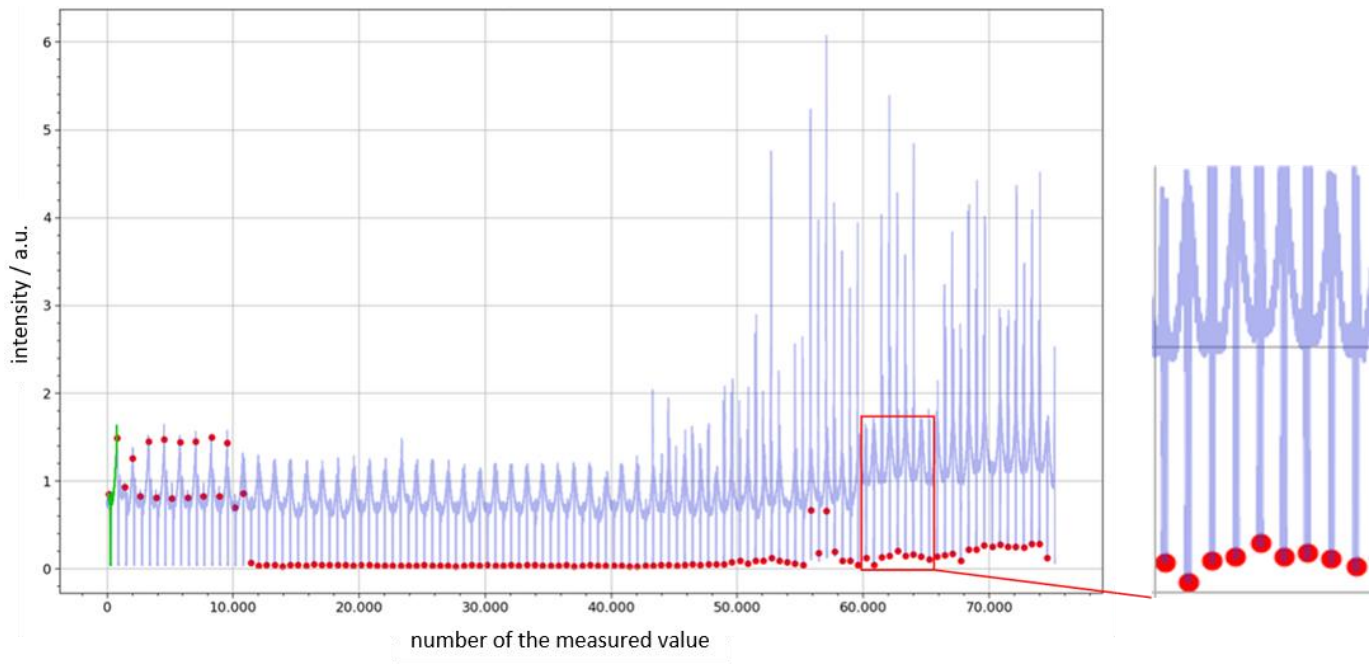

Figure 11. FRS measurement with cloud entry and shutter test. Briefly closing the laser shutter enables the background measurement. Two spectra per second are recorded and the background in between.

4. Conclusion and outlook

A successful in-flight application of filtered Rayleigh scattering was demonstrated up to about 9000 m height providing temperature estimates at a rate of 2 Hz. For straight ahead flights at constant height, temperature mean values were in good agreement with the flight data system of the DLR research aircraft Dassault Falcon 20 (D-CMET). But the accuracy required for flight data systems (~ 0.5 K) has not yet been achieved. The scatter of the single sweep temperature data from the FRS system was analysed. The FRS measurement system was presented, application aspects and improvements discussed.

The signal levels achieved indicate that measurements should also be possible at even higher altitudes. However, the signal strength of FRS signal in comparison to bright background conditions such as bright sunlight or sun back-scatter from the top of clouds must be further improved in order to be able to provide reliable measurements in these conditions. On the one hand, this can be achieved with a further improved fast shutter concept. On the other hand, significantly stronger FRS signals could be generated in the ultraviolet spectral range due to the larger scattering cross-section and strongly reduced spectral contribution by sunlight. While the wavelength of 532 nm used here is close to the maximum radiation intensity of the sun, the radiation intensity in the ultraviolet spectral range is orders of magnitude lower. This is amplified

by ozone absorption in the upper atmosphere. The chosen wavelength should be above the onset of O_2 absorption (~ ≥ 242 nm), e.g. at about 253.7 nm for which mercury vapor filters could be used in place of the iodine cells used in the present setup [Miles et al. 2001] (compare also [Witschas 2021]).

As the three mentioned measurement systems were operated in a synchronized manner [Kliebisch et al. 2023], acquired data can be used in an augmented fashion to improve overall measurement uncertainties. In particular, the vertical velocity component provided by the LDA system could be used to fix the Doppler shift parameter in the FRS multi-parameter fit. In a similar manner, the optically deduced pressure provided by the TDLAS system can further reduce the number of fitting parameters which leads to a reduction of the scatter of the FRS temperature and systematic errors. This illustrates how the coupled optical systems can benefit from each other in a future "optical air data system" (OADS) for commercial aircraft.

Acknowledgments

The work presented was mainly funded by the DLR internal project FAME. The development of the measurement methodology was partly funded by the German LuFo V-3 program (grant label 20Q1729C). The support of Andreas Fix (DLR-PA), Andre Schmitt (DLR-TP) and Georg Dietz (DLR FX-PMF OP) is gratefully acknowledged.

References

Cao, Y., Tan W., & Wu Z. (2018). Aircraft icing: An ongoing threat to aviation safety, Aerospace Science and Technology, 75, 353-385. https://doi.org/10.1016/j.ast.2017.12.028

Doll, U. (2016). Gefilterte Rayleigh-Streuung zur simultanen Bestimmung von Druck-, Temperatur- und Geschwindigkeitsfeldern in Gasströmungen. PhD Thesis, TU Dresden, Germany.

Doll, U., Fischer, M., Stockhausen G., & Willert, C. E. (2012). Frequency scanning filtered Rayleigh scattering in combustion experiments. In 16'th Int. Symposium on Applications of Laser Techniques to Fluid Mechanics, Lisbon, Portugal.

FAME, DLR internal project, "Future Air Data System Module Evaluation".

Fischer, M., Stockhausen, G., Burow, E., Beversdorff, M., & Chacin Krist, A. (2024), Development of a Single Point Frequency Sweeping Filtered Rayleigh Scattering Method and Probe. To be submitted to Optics Letters.

Forkey, J., Finkelstein, N., Lempert, W., & Miles, R. (1996). Demonstration and characterization of filtered Rayleigh scattering for planar velocity measurements. AIAA Journal, 34 (3), 442-448.

Jagodzinski, J. J. (2007). A Diode Laser-Based Velocimeter Providing Point Measurements in Unseeded Flows Using Modulated Filtered Rayleigh Scattering (MFRS). PhD Thesis, The University of Texas at Austin.

Jungmann, J. (2019). Entwicklung und Charakterisierung einer Sonde auf Basis der gefilterten Rayleigh-Streuung für zeitaufgelöste Messungen unter kryogenen Bedingungen. Master Thesis, German Aerospace Center (DLR), Institute of Propulsion Technology, Cologne and University of Technology, Cologne.

Jäckel, R., Gutiérrez-Urueta, G., & Tapia, F. (2021). A review on Pitot tube icing in aeronautics: Research- design and characterization – future trends, Flow Measurement and Instrumentation, 81, 102033. https://doi.org/10.1016/j.flowmeasinst.2021.102033

Kliebisch, O., Mahnke, P., Lorbeer, R. A., Damm, M., Burow, E. J., Fischer, M., Beversdorff, M., Stockhausen, G., Dietz, G., Fuchs, T., & Burwitz, S. (2023). Flight testing of three laser-optical techniques for future optical air data sensors. Presentation, Deutscher Luft- und Raumfahrt Kongress, (DLRK), September 19. -21., Stuttgart, Germany.

Kliebisch, O., Mahnke, P. & Damm, M. (2023). Airborne test of a vector laser Doppler anemometer as true airspeed, angle of attack, and angle of sideslip sensor. European Test & Telemetry Conference. June 13.-14., Toulouse, France.
LDA_ETTC2023_Conference_Paper.pdf (dlr.de)

Lemmon, E. W. & Jacobsen, R. T. (2004). Viscosity and Thermal Conductivity Equations for Nitrogen, Oxygen, Argon, and Air. International Journal of Thermophysics, 25(1), 21-69.

Miles, R. B., Lempert, W. R. & Forkey, J. N. (2001). Laser Rayleigh scattering. Measurement

Science and Technology, 12(5), R33 (review article).

Powers, S., Byun, G., & Lowe, K. T. (2022). Auto-Processing of Filtered Rayleigh Scattering Images Including Mie and Background Scattering Contributions. Preprint on Research Square. https://doi.org/10.21203/rs.3.rs-2370966/v1

Witschas, B. (2011). Experiments on spontaneous Rayleigh-Brillouin scattering in air. PhD Thesis (in English), Friedrich-Schiller-University, Jena, Germany.

Witschas, B., Lemmerz, C., Lux, O., Marksteiner, U., Reitebuch, O., & Schäfler, A. (2021). Airborne temperature profiling in the troposphere during daytime by lidar utilizing Rayleigh–Brillouin scattering. Optics Letters, 46 (17), 4132 – 4135.